

# Using Chiral Auxiliaries to Mimic the Effect of Chiral Media on the Structure of Lanthanide(III) Complexes Common in Bioimaging and Diagnostic MRI

Lea Gundorff Nielsen,<sup>a</sup> Helene O. B. Andersen,<sup>a</sup> Alan M. Kenwright,<sup>b</sup> Carlos Platas-Iglesias<sup>c</sup> and Thomas Just Sørensen<sup>\*a</sup>

<sup>a</sup> Department of Chemistry & Nano-Science Center, University of Copenhagen, Universitetsparken 5, DK2100 København Ø, Denmark. [tjs@chem.ku.dk](mailto:tjs@chem.ku.dk)

<sup>b</sup> Department of Chemistry, Durham University, South Road, Durham, United Kingdom, DH1 3LE

<sup>c</sup> Universidade da Coruña, Centro Interdisciplinar de Química e Bioloxía (CICA) and Departamento de Química, Facultade de Ciencias, 15071, A Coruña, Galicia, Spain.

**ABSTRACT:** [Ln·DOTA]<sup>-</sup> complexes, and systems derived therefrom, are commonly used in MRI and optical bioimaging. These lanthanide(III) complexes are chiral and, in solution, they are present in four forms, with two sets of enantiomers, with the ligand backbone in either a square antiprismatic, SAP, or twisted square antiprismatic geometry, TSAP. This complicated speciation is found in laboratory samples. To investigate speciation in biological media, when Ln·DOTA-like complexes interact with chiral biomolecules, six Eu·DOTA-monoamide complexes were prepared and investigated using 1D and 2D <sup>1</sup>H NMR. To emulate the chirality of biological media, the amide pendant arm was modified with one or two chiral centers. It is known that a chiral center on the DOTA scaffold significantly influences the properties of the system. Here, it was found that chirality much further away from the metal center changes the available conformational space, and that both chiral centers and amide cis/trans isomerism may need to be considered. A fact that, for the optically enriched materials, led to the conclusion that eight chemically different forms may need to be considered, instead of the four forms necessary for DOTA. The results reported here clearly demonstrate the diverse speciation that must be considered when correlating an observation to a structure of a lanthanide(III) complex.

## Introduction

Kinetically inert lanthanide(III) complexes based on ligands derived from cyclen and TACN have been used in many forms of bioimaging and diagnostics.<sup>1-13</sup> Less stable DTPA, cryptands, and siderophore-based ligand systems are also prevalent.<sup>14, 15</sup> A common denominator in many of these systems, especially the macrocyclic systems, is that they adopt several forms with different chirality in solution.<sup>16-20</sup> However, when a chiral agent is added, the equilibrium between the different isomers may be perturbed.<sup>11, 21-25</sup> This is important, as biological systems are inherently chiral. Any use of these lanthanide(III) complexes in biological applications will either favor a specific form or create a number of new forms by interaction between two or more molecules with more than one chiral element.<sup>9, 12, 26</sup> The inherent chirality of biomolecules was recently used by Parker to develop responsive molecules. Using the rigid TACN macrocycle, complexes were achieved with a resolved chirality, and the specific handedness controlled the binding of the complex to specific biomolecules.<sup>9</sup>

Here, we have mimicked the influence of biological chirality by adding additional chiral elements to the lanthanide complex itself. Specifically, ligand systems were made

with diastereomeric pendant arms. The resulting kinetically inert lanthanide(III) complexes thus contained four chiral elements.

Due to the development of gadolinium(III) based MRI contrast agents, these systems have been extensively studied to optimize and control the relaxivity and stability of these Gd(III) complexes.<sup>3, 18, 27</sup> Small structural perturbations, such as enforced control of conformational space, have been shown to dramatically influence these properties.<sup>3, 11, 28-35</sup> Steric effects of adding extra substituents can be used to favor specific conformations and prevent either ring inversion or side-arm rotation.<sup>3, 31, 34, 36-38</sup> Introduction of a *p*-NO<sub>2</sub>-benzyl group in the macrocycle has been shown to lock the conformation of the cyclen ring thus resulting in only two conformations present.<sup>36</sup> Methyl groups in the  $\alpha$  position of all the pendant arms have been shown to prevent side-arm rotation, as in the complexes of DOTMA.<sup>31, 34, 37</sup> By combining these effects in efforts to investigate the relationship between conformation, chirality and the physicochemical properties of lanthanide(II) complexes, systems with only one conformation have been made and used to show strong dependencies between relaxometric properties and structure.<sup>11, 35</sup> Thus, it must be anticipated that the structural perturbations induced by a chiral environment can have dramatic effect on these complexes.



**Scheme 2. General synthesis of *t*-Bu protected DO3A type ligands, 7-10.**

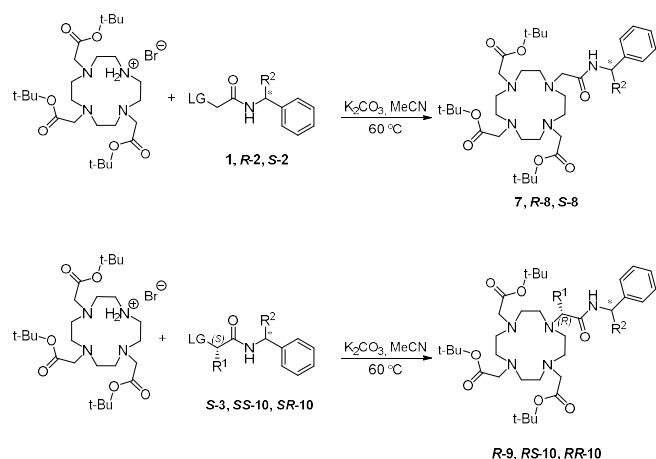


**Table 1: Reaction times, yields and purification methods for pre-ligands 7-10.**

Amide	R <sub>1</sub>	R <sub>2</sub>	Product	Reaction time	Purity %	Yield %
1	H	H	7	4 h	>94	>85
R-2	H	R-Me	R-8	4 h	>94	>81
S-2	H	S-Me	S-8	4 h	>92	>38
S-3	Me	H	R-9	24 h	>93	>68
SR-4	Me	R-Me	RR-10	24 h	>93	>75
SS-4	Me	S-Me	RS-10	24 h	>93	>48

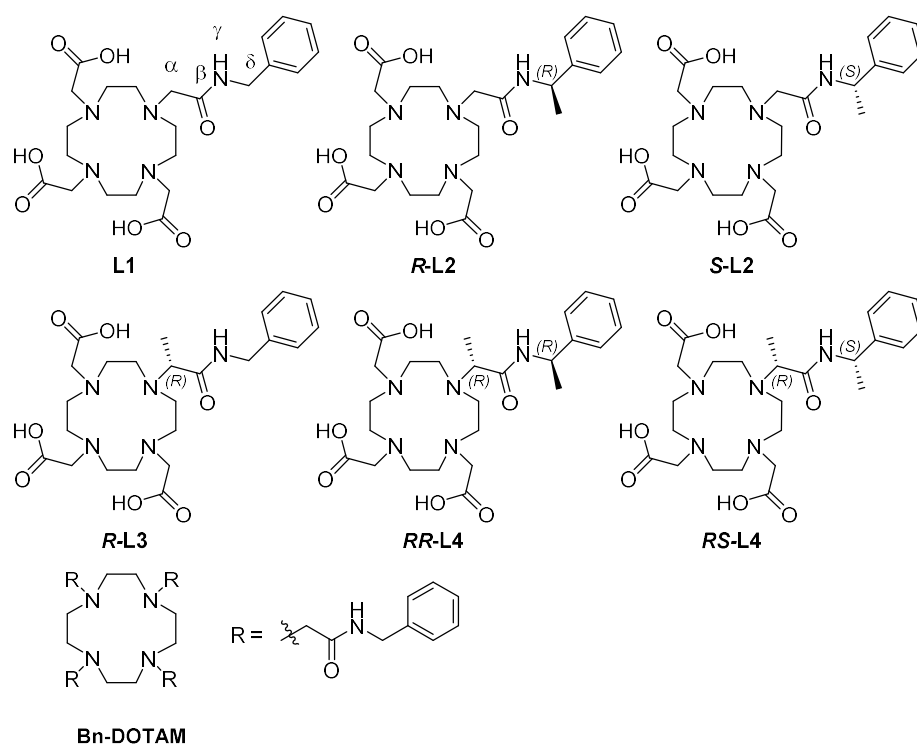


**Figure 2:** Amide appended DO3A type ligands used in this work for complexation with Eu(III). The pendant arms differ in the number of chiral centers.

In the synthesis of **S-2** the reaction time was reduced to 3 h maintaining the high yield. We noted that the longer reaction time in the case of **R-2** resulted in formation of a red side product, which was not observed in the synthesis of **S-2**. The two compounds are enantiomers and this is reflected in the identical NMR spectra, see Figures S11-12.

The first step towards the electrophiles **S-3**, **SR-4** and **SS-4** was the synthesis of the corresponding hydroxyl precursors **S-5**, **SR-6** and **SS-6**, see Scheme 1. These were synthesized from the commercially available ethyl ester of *S*-lactic acid and the appropriate amine following literature procedures.<sup>47</sup> The diastereomeric nature of **SR-6** and **SS-6** can be observed in the NMR spectra, see Figures S17 and S19. Unlike the enantiomeric couple of **R-2** and **S-2**, the spectra are different, and we see no products of racemization, which

will lead to the formation of a set of two diastereoisomers with new resonances. As only one product is observed in the NMR spectra, it can be concluded that only insignificant racemization has occurred. As no significant inversion of the stereocenter was observed in the synthesis of **SR-6** and **SS-6** it is assumed that any inversion that takes place in the synthesis of **S-5** can be ignored. Compound **S-3** is a known compound and was synthesized following literature procedures.<sup>45</sup> Compounds **SR-4** and **SS-4** were synthesized in a similar manner, where the hydroxy-groups were converted to the mesylate by addition of mesyl chloride in the presence of base in DCM at low temperature.

The reported purification process is column chromatography.<sup>45</sup> However, it was found that filtration through a small plug of silica was sufficient to obtain the pure product. This was done for **R-3** and **SR-4**. Compound **SS-4** was purified by precipitation from EtOAc and heptane, which gave the pure product but in lower yield. The diastereomeric nature of compounds **SR-4** and **SS-4** is apparent in the NMR spectra, see Figure S23 and S25. No signs of racemization products are observed for **SR-4** and **SS-4** in the respective NMR spectra, and it is therefore again assumed that if racemization occurs in the synthesis of **S-3**, it is insignificant. Introduction of the amide arms to the *tert*-butyl protected DO<sub>3</sub>A was done following the typical procedures for alkylation of DO<sub>3</sub>A.<sup>45, 48, 49</sup> The reaction times are given in Table 1.

The reactions are expected to go via an S<sub>N</sub>2 mechanism resulting in inversion of the α-stereocenter. This should result in the *R* configuration of products **9-10**. Bulky nucleophiles however favor S<sub>N</sub>1 reactions and as *tert*-butyl protected DO<sub>3</sub>A is relatively bulky it should be considered whether the reaction goes purely via an S<sub>N</sub>2 mechanism or if some S<sub>N</sub>1 reactions are taking place. Scheme 2 shows the formation of **7-8** where the mechanism does not matter, as there is no stereocenter at the site of substitution. However, compounds **9-10** will show scrambling of the stereocenter at the site of attack if the mechanism is S<sub>N</sub>1, see Scheme 1. If this is the case, compounds **RR-10** and **RS-10** will show formation of two diastereoisomers. MALDI-TOF analysis was used to follow the progress of the reactions. It was found that introduction of a chiral center in the α position on the pendant arm lead to longer reaction times. In the formation of **7** no starting material was observed after only 1 hour but for **RS-10** the starting material is still largely present after 3 h. Extending the reaction time to 24 h led to full conversion of the starting material. The increased reaction time is due to steric effects as the secondary carbon of the mesylate is more hindered towards nucleophilic attack by the amine of the DO<sub>3</sub>A triester. The reaction time was adapted accordingly.

To ensure that no scrambling of the α position stereocenter occurred in compounds **9-10** the <sup>1</sup>H-NMR at 27 °C of **RR-10** and **RS-10** was scrutinized (Figure S33 and Figure S35). As one proton gives rise to multiple signals, it could appear that some scrambling did take place. However, each proton gives rise to three distinct resonances, most clearly from the δ-proton at 5 ppm, while scrambling of the stereocenter only would give rise to two distinct resonances.

Figure 3 shows variable temperature (VT) <sup>1</sup>H-NMR experiments of **RR-10** in DMSO-*d*<sub>6</sub>. The data reveal that the resonances are in exchange and the different species present must be a result of different conformations in slow exchange on the NMR timescale, not two diastereomers. The signals move together upon heating, almost reaching the coalescence temperature at 87 °C. This observation is most clearly seen in the resonances from the amide and δ protons. Note that VT <sup>1</sup>H-NMR experiments of **Y-L4** and **Lu-L4** in DMSO-*d*<sub>6</sub> are included in Figure 3 to show that the exchanging conformations are also found in the complexes of **RR-10**.

The final step in the synthesis is deprotection of the preligands and complexation of the ligands with europium(III). The deprotection was performed with TFA and with hydroxides to verify that no scrambling of the chiral centers could be observed in the NMR data, see the supporting information for details. The complexes were achieved using the Eu(III) triflate salt (Eu(OTf)<sub>3</sub>) and purification using cation exchange columns.

#### The four ligands studied

The complexes of **Eu-L4** are used to model the effects that biological media impose on simple [Eu-DOTA]-like complexes in solution. For **Eu-L1**, with no additional chirality, only resonances from the two sets of enantiomers are expected and observed. To mimic the influence of associating a diastereomeric biomolecule with **Eu-L1**, **Eu-L4** was used where chirality can be either *RR* or *RS*. **Eu-L2**, and **Eu-L3** were used to investigate if the complexity observed for **Eu-L4** is caused by the changes in chirality.

#### Solution structure of **Eu-SR-4** and **Eu-RR-L4**

The complexes **Eu-SR-4** and **Eu-RR-L4** contain at least four chiral units in the form of the two chiral centers on the pendant arm and the DO<sub>3</sub>A-monoamide europium(III) complex shown in Figure 1B. For a DO<sub>3</sub>A type or DOTA-monoamide complex, with no additional chirality, ring inversion and arm rotation leads to four forms in two enantiomeric pairs. Thus, only two sets of signals—from the SAP and from the TSAP forms respectively—are observed for simple achiral complexes, while four sets will be resolved by adding a chiral auxiliary like the pendant arm **4**.

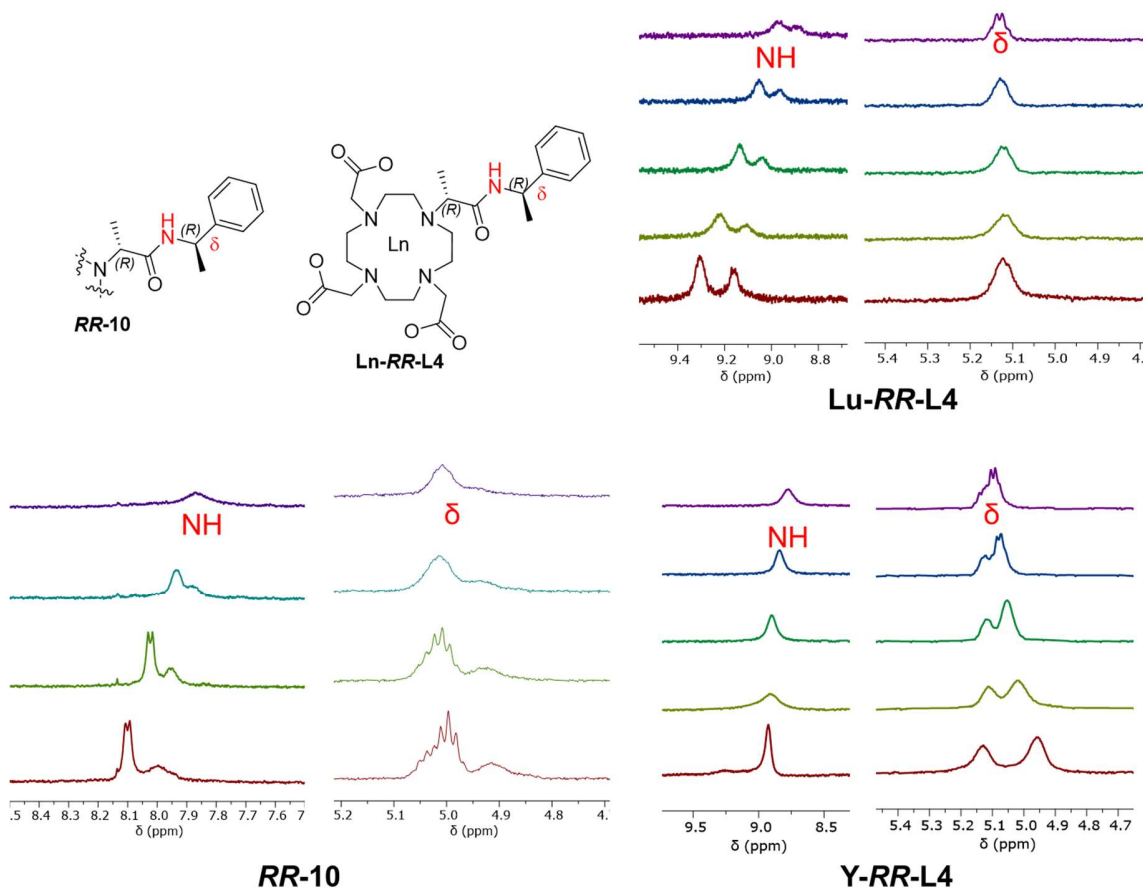


**Figure 3.**  $^1\text{H-NMR}$  spectrum of **RR-10**, **Lu-RR-L4**, and **Y-RR-L4** in  $\text{DMSO-d}_6$  at variable temperatures ( $\sim 20$  -  $\sim 80$   $^\circ\text{C}$ ) in the amide and  $\text{H}_\delta$  regions.

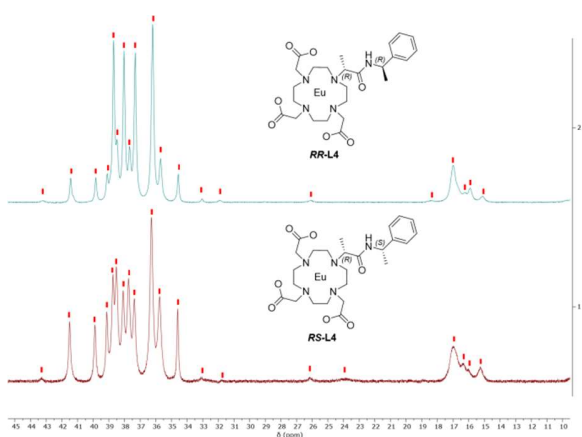


**Figure 4.**  $^1\text{H-NMR}$  spectra of **Eu-RR-L4** in  $\text{MeOH-d}_4$  (top) and of **Eu-RS-L4** in  $\text{MeOH-d}_4$  (bottom) showing the region from 10-45 ppm. Peaks are indicated by the red squares to indicate the number of forms.

Unexpectedly, at least five diastereomeric forms (20 resolved peaks) present and in slow exchange were observed in the  $^1\text{H-NMR}$  spectra of the paramagnetic  $\text{Eu(III)}$  complexes of ligands **RR-L4** and **RS-L4** reported in Figure

4. Other systems with similar conformational freedom to adopt both *E* and *Z* forms of the amides have been reported in literature.<sup>50, 51</sup> Building on our understanding of  $[\text{Eu}\cdot\text{DOTA}]^-$  NMR,<sup>19, 42, 52-54, 53, 55</sup> we can see that the spectra show three to four forms with a SAP geometry and at least two with a TSAP geometry. Thus, the four forms known to describe the conformation chemistry of  $[\text{Ln}\cdot\text{DOTA}]^-$  are not enough to describe the forms of **Eu-RR-L4** and **Eu-RS-L4**. Additional forms changing either the chemical or the magnetic environment must be considered, in addition to the exchange between two SAP and two TSAP forms. We propose that additional conformations are present and these conformations may occur due to the stereochemistry of the amide bond, which is exchanging between the *E* or *Z* configuration. Amide bond rotation would increase the number of conformations in slow exchange from four to eight as illustrated in Figure 5. Note that  $^1\text{H}$  NMR spectra recorded in  $\text{DMSO-d}_6$  and  $\text{D}_2\text{O}$  contained the same information, and that adding in excess of 10 mol% of water/ $\text{D}_2\text{O}$  to  $\text{DMSO-d}_6$  does not reduce the complexity of the spectra, see Figures S101 and S102 for details. Further, under the addition of  $\text{H}_2\text{O}$  to the NMR sample at least two exchangeable signals appeared that are not present with  $\text{D}_2\text{O}$  added, see Figure S104 and S105.

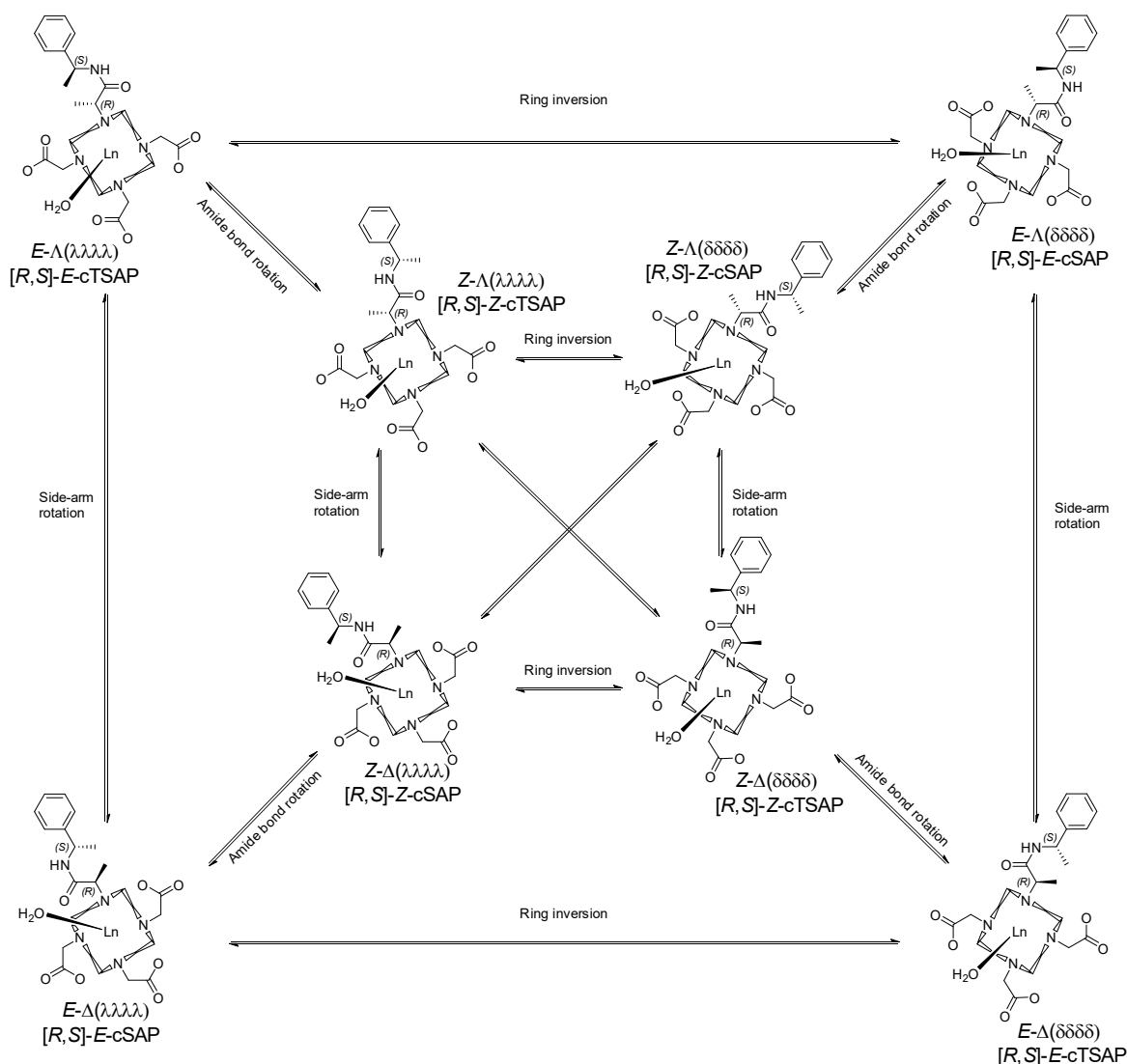


**Figure 5.** Possible conformations and exchange processes suggested for the  $\text{Ln}\cdot\text{L}_4$  complexes including slow amide bond rotation, shown for  $\text{Ln}\cdot\text{RS}\text{-L}_4$ . Note that the capping solvent, here shown as water, will be that used in the experiment: MeOH, DMSO or water.

For both Eu(III) complexes the major form has the SAP geometry. In the spectra of  $\text{Eu}\cdot\text{RR}\text{-L}_4$  one SAP form is clearly dominant, while in the spectra of  $\text{Eu}\cdot\text{RS}\text{-L}_4$  two SAP forms appear equally populated. Both spectra in Figure 4 show the presence of two forms with TSAP geometry with very broad peaks suggesting a distorted TSAP form. Note that this is also observed in  $\text{DSMO-d}_6$ , see Figure S10i.

#### $2\text{D}$ NMR of $\text{Eu}\cdot\text{SR}\text{-L}_4$ and $\text{Eu}\cdot\text{RR}\text{-L}_4$

To support the proposed model in Figure 5, we turned to  $2\text{D}$  EXSY spectra. These show cross peak correlations between resonances from forms in exchange, allowing observation of correlations between the two signals from the different forms in the  $1\text{D}$  spectrum. The cross peak correlations expected from the SAP conformation of  $[\text{Eu}\cdot\text{DOTA}]^-$  are given in Table 2.

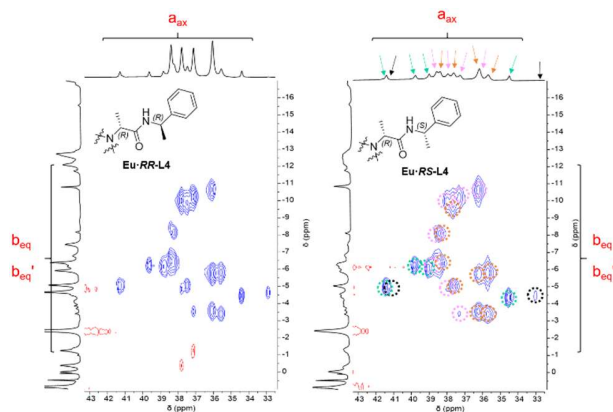
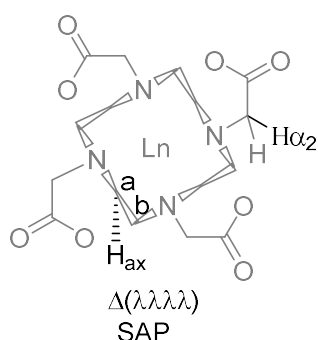


**Figure 6.**  $2\text{D}$  EXSY spectra of  $\text{Eu}\cdot\text{RR}\text{-L}_4$  (left) and  $\text{Eu}\cdot\text{RS}\text{-L}_4$  (right) in  $\text{MeOH-d}_4$  with 12 ms mixing time. The spectra show the  $a_{\text{ax}}$  region

Figure 6 shows the  $a_{ax}$  region of the 2D EXSY spectra obtained from **Eu-RR-L4** and **Eu-RS-L4** (The full 2D spectra are reported in Figures S97-98). For achiral non-symmetrical DOTA and DO<sub>3</sub>A type complexes two sets of four signals (8 signals) would be expected in the  $a_{ax}$  proton region arising from the SAP and TSAP conformations. However, for **Eu-RR-L4** and **Eu-RS-L4** at least 14 signals are resolved indicating the presence of four sets of four signals in the  $a_{ax}$  proton region, see Figure 6. This is consistent with the proposed model that includes slow amide bond rotation in addition to side-arm rotation and ring inversion, see Figure 5.

**Table 2: Cross peak correlations that will be observed in a 2D EXSY spectrum for the SAP conformation of a [Ln·DOTA]<sup>-</sup> complex. The letters a/b are in SAP and a'/b' are in TSAP.**



Process	Cross peaks					
	$a_{ax}$	$a_{eq}$	$b_{eq}$	$b_{ax}$	$\alpha 2$	$\alpha 1$
Side-arm rotation	$a_{ax}'$	$a_{eq}'$	$b_{eq}'$	$b_{ax}'$	$\alpha 1'$	$\alpha 2'$
Ring Inversion	$b_{eq}'$	$b_{ax}'$	$a_{ax}'$	$a_{eq}'$	$\alpha 2'$	$\alpha 1'$
Side-arm rotation + ring inversion	$b_{eq}$	$b_{ax}$	$a_{ax}$	$a_{eq}$	$\alpha 1$	$\alpha 2$

For **Eu-RS-L4** two sets of signals are marked with pink and orange in Figure 6. These show two cross peaks in the  $b_{eq}$  area and no cross peaks to the  $a_{ax}$  TSAP protons. The resonances marked with green and black in Figure 6 only have one cross peak to the  $b_{eq}$  protons, but have cross peaks between the  $a_{ax}$  and  $a_{ax}'$  protons. Finally, the distorted TSAP form shows no cross peaks. The cross peaks for the pink and orange sets thus arise from ring inversion ( $a_{ax} \leftrightarrow b_{eq}'$ ) and combined side-arm rotation and ring inversion ( $a_{ax} \leftrightarrow b_{eq}$ ), while the cross peaks for the sets marked with green and black arise from side-arm rotation ( $a_{ax} \leftrightarrow a_{ax}'$ ) and combined side-arm rotation and ring inversion ( $a_{ax} \leftrightarrow b_{eq}'$ ). Amide bond rotation will lead to exchange between two  $a_{ax}$  protons, but no cross peak correlations are observed for such an exchange. However, amide bond rotation is typically slow, and cross peaks corresponding to this exchange

process is not expected in the 2D EXSY spectra. Therefore, we only expect to see the cross peaks for each signal as for [Eu·DOTA]<sup>-</sup>, but with up to eight resolved forms, which is consistent with the observed spectra.

Variable temperature studies were done on diamagnetic complexes of **Y-RR-L4** and **Lu-RR-L4** to support the hypothesis of slow amide bond rotation, see Figure 3. It was found that the amide bond rotation is much slower than exchange between SAP and TSAP. Thus, the amide bond rotation would be too slow to observe cross peaks in the 2D EXSY spectra with a mixing time of 12 ms.

It should be considered whether the observation of eight conformations in the spectra of the **Ln-L4** complexes is a result of racemization at the  $\alpha$  stereocenter, as this would lead to two species with four forms in slow exchange. This would also explain the observation of eight sets of peaks in the paramagnetic spectra. However, no indication of racemization was observed in the synthesis, and variable temperature studies of the **Y-RR-L4** and **Lu-RR-L4** are compatible with exchange between amide bond rotation, suggesting that racemization is not the origin of eight conformations. As racemization is unlikely, amide bond rotation appears to be a plausible explanation for the observed complicated solution state dynamics. The amide *E/Z*-stereoisomerism, combined with the diastereomeric nature of the arms in **Eu-RR-L4** and **Eu-RS-L4**, illustrate the change in properties of a DOTA-like lanthanide complex when interacting with a protein surface. The changes in properties are here illustrated through the NMR spectra, and the effect can be seen by comparing the complexity in the NMR spectra in Figures 4 and 7.

DFT calculations were performed to provide further support to the exchange processes assigned in the NMR analysis above, see Supporting Information for the computational details. We optimized the structure of the [R,R]-Z-cSAP and [R,R]-E-cSAP isomers of the **Eu-RR-L4** complex, and subsequently optimized the transition state involved in the *Z* ↔ *E* interconversion process. These calculations afforded an activation Gibbs free energy of  $\Delta G^\ddagger = 91.2 \text{ kJ mol}^{-1}$  at 298 K. This value is significantly higher than those reported for arm-rotation and ring-inversion process in DOTA derivatives.<sup>56-58</sup> The time-scale of the amide-bond rotation processes can be estimated from the value of  $\Delta G^\ddagger$  using the Eyring equation, which affords a  $k^{298}$  value of  $6.5 \times 10^{-4} \text{ s}^{-1}$ . These results suggest that the amide-bond process is in the minute time-scale at 298 K, which is in line with the NMR data where 12 ms EXSY timescale did not show this process. In contrast, the value of  $\Delta G^\ddagger$  obtained with DFT for the arm rotation process is  $51.0 \text{ kJ mol}^{-1}$ , which indicates that arm rotation takes place in the  $\mu\text{s}$  –  $\text{ms}$  time-scale accessible by NMR ( $k^{298} = 4215 \text{ s}^{-1}$ ). One interesting aspect is that the arm-rotation process in this complex follows the concerted mechanism involving simultaneous rotation of the four pendant arms. This is in agreement with previous computational studies performed for lanthanide DOTA complexes.<sup>56, 59, 60</sup> Similarly, and in agreement with previous works,<sup>56, 59, 60</sup> ring inversion takes place stepwise,

where each step involving a  $\delta \leftrightarrow \lambda$  interconversion process.<sup>56, 59-61</sup> The value of  $\Delta G^\ddagger$  for the ring-inversion process was estimated from the transition state with the highest energy as  $\Delta G^\ddagger = 76.1 \text{ kJ mol}^{-1}$  at 298 K. This value is somewhat higher than those determined experimentally and computationally for different DOTA derivatives ( $\sim 65 \text{ kJ mol}^{-1}$ ),<sup>61</sup> which suggests that the presence of a bulky amide group attached to the macrocyclic structure hinders the ring-inversion process to a certain extent. Finally, rotation about the amide HN—CHMePh single bond was characterized by a low  $\Delta G^\ddagger$  value of  $22.1 \text{ kJ mol}^{-1}$  at 298 K, and thus is too fast to play any role in the exchange processes evidenced by NMR.

### Reducing the number of chiral elements

With the effects of chirality documented for the model system, we turn to the parent compounds to scrutinize the effect of the *E/Z* forms of the amide bond. The solution structures of the symmetric  $[\text{Eu}\cdot\text{DOTA}]^-$  and  $[\text{Eu}\cdot\text{Bn-DOTAM}]^{3+}$  is explored to support the observations and assumptions made above, before we turn to the less simple DOTA-monoamide complexes.

The paramagnetic  $^1\text{H-NMR}$  spectra of  $[\text{Eu}\cdot\text{DOTA}]^-$  and  $[\text{Eu}\cdot\text{Bn-DOTAM}]^{3+}$  are shown in Figure S91 and Figure 7 respectively. Both spectra are consistent with spectra reported in literature.<sup>52, 62</sup>

The 2D EXSY spectrum of  $[\text{Eu}\cdot\text{DOTA}]^-$  (Figure S91) shows three cross peak correlations for each peak consistent with the expected three exchange processes shown in Table 2. The 2D EXSY spectrum of  $[\text{Eu}\cdot\text{Bn-DOTAM}]^{3+}$  is shown in Figure 7. Here, four cross peak correlations are observed for each signal. This is surprising as we expect the complex to behave like the  $[\text{Eu}\cdot\text{DOTA}]^-$  complexes and thus give rise to the same three cross peak as  $[\text{Eu}\cdot\text{DOTA}]^-$ . The three expected exchange processes are marked with blue, green and red in Figure 7.

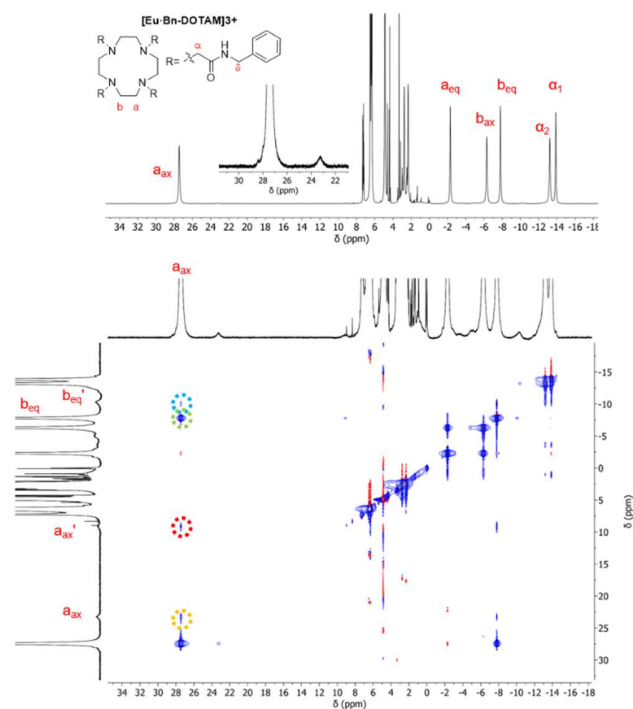


**Figure 7.** Paramagnetic  $^1\text{H-NMR}$  spectra of  $[\text{Eu}\cdot\text{Bn-DOTAM}]^{3+}$  in  $\text{MeOH-}d_4$  (top) and paramagnetic 2D EXSY spectrum of  $[\text{Eu}\cdot\text{Bn-DOTAM}]^{3+}$  in  $\text{MeOH-}d_4$  with 12 ms mixing time (bottom). The cross peaks marked corresponds to the following exchange processes: ring inversion (blue), side-arm rotation + ring inversion (green) and side-arm rotation (red).

The additional peak is marked with orange, corresponds to a fourth exchange process between two protons occupying the  $a_{ax}$  position in a SAP conformation. This suggests that an additional SAP conformation is present. Unlike the cycle between the usual SAP and TSAP conformations that gives three cross peaks, it appears that this conformation can only return to the SAP conformation through the same path that it was formed. The proposed amide bond rotation of the SAP isomer would lead to an  $a_{ax} \leftrightarrow a_{ax}$  cross peak correlation as is observed, see Figure 5, i.e. the two SAP forms could be present due to *E/Z* isomerism in one of the amide bonds. The 2D EXSY spectrum of  $[\text{Eu}\cdot\text{Bn-DOTAM}]^{3+}$  thus support the observation that the normal scheme used to describe  $[\text{Eu}\cdot\text{DOTA}]^-$  is not adequate to describe the solution state structure and dynamics of DOTA-amides as an additional exchange process takes place.

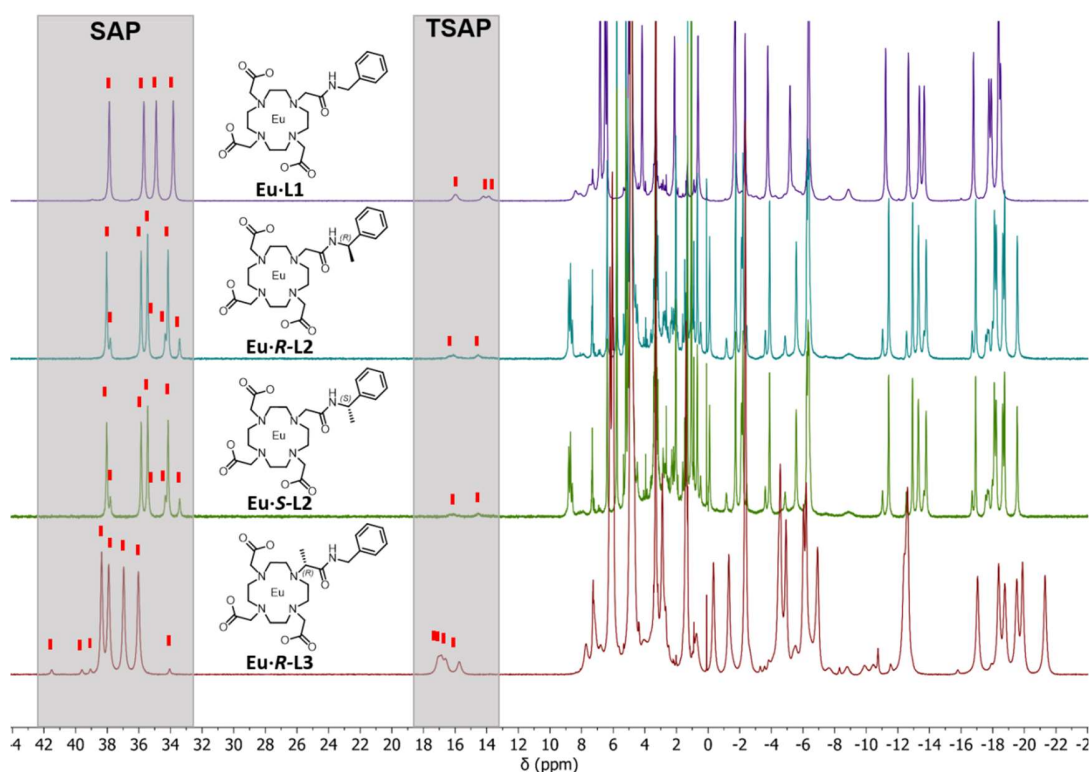


**Figure 8.**  $^1\text{H-NMR}$  spectra of **Eu-L1** (purple), **Eu-R-L2** (blue), **Eu-S-L2** (green) and **Eu-R-L3** (red) in  $\text{MeOH-}d_4$ . SAP and TSAP regions marked with grey. Different forms are marked with red squares in the SAP and TSAP region.

The amide bond rotation may be important in the sterically congested DOTA-tetramides, but that may not be the case in DOTA-monamides. The lower symmetry of these systems results in a larger number of signals. The  $^1\text{H-NMR}$  spectrum of achiral but unsymmetrical **Eu-L1** only shows one major and one minor isomer present, with the major isomer being in the SAP geometry (Figure S59). For **Eu-L1** the paramagnetic 2D EXSY spectrum shows only the three cross peak correlations for each proton we know from  $[\text{Eu-DOTA}]^-$ ,<sup>52</sup> and no exchange corresponding to amide rotation was observed.

#### Analysis of chiral **Eu-R-L2**, **Eu-S-L2** and **Eu-R-L3**

Figure 8 includes the  $^1\text{H-NMR}$  spectrum of achiral **Eu-L1**. The introduction of chiral centers in the ligand structure complicates the NMR as the two SAP and the two TSAP forms are no longer enantiomers, which increases the number of diastereomeric forms from two to four. For the enantiomeric pair of paramagnetic complexes **Eu-R-L2** and **Eu-S-L2**, introduction of a chiral center in the  $\delta$  position thus resolves the four forms in the two identical  $^1\text{H-NMR}$  spectra, see Figure 8. In these spectra four additional resonances in the SAP region (32–44 ppm) are readily observed. cursory inspection of the 2D EXSY spectra of **Eu-R-L2** in Figure 9, confirms that there are two sets of four signals from the SAP forms. These are marked with black and orange circles. The 2D EXSY spectrum of **Eu-R-L2** shows three cross peak correlations for each proton, corresponding to ring inversion ( $a_{\text{ax}} \rightleftharpoons b_{\text{eq}}$ ), side-arm rotation ( $a_{\text{ax}} \rightleftharpoons a_{\text{ax}'}$ ) (see Figure S94) and a combination of the two ( $a_{\text{ax}} \rightleftharpoons b_{\text{eq}}$ ).<sup>52</sup> As all three expected cross peaks are observed, the

two SAP forms are in exchange with two TSAP forms and the 2D spectrum confirms the presence of the two TSAP forms. Thus, all four possible  $[\text{Ln-DOTA}]^-$  conformations are present in solution.

The relative intensities in the 1D spectra show that one SAP conformation is dominating. As the *R* configuration favors the  $\Lambda$  helicity and the *S* configuration favors  $\Delta$  helicity of the arms, we expect the major forms present to be  $\Lambda(\delta\delta\delta\delta)$  for **Ln-R-L2** and  $\Delta(\lambda\lambda\lambda\lambda)$  for **Ln-S-L2**.<sup>63,64</sup> One specific orientation of the pendant arms is more favored for these complexes, as the presence of a chiral center in the  $\delta$  position favors a single orientation of the side-arms. Note that the amide bond rotation is not resolved/not a factor in the spectra of **Eu-L2**.

Figure 8 also shows the NMR spectrum of **Eu-R-L3**. This complex has a chiral center in the  $\alpha$  position and also shows four non-equivalent forms in solution. Due to the chirality of the complex, two distinct set of signals are observed in the SAP region, indicating that two SAP geometries are present.<sup>49, 65</sup> The dominating form has a SAP geometry, while in contrast to **Eu-L2**, the second most intense peaks arise from a TSAP form. Thus, moving the chiral center closer to the cyclen ring (**L3**) changes the observed shifts and changes the proportion of SAP/TSAP. For the major form of **Eu-R-L3** the 2D EXSY spectrum shows two sets of cross peaks from the axial SAP protons. Only one set of cross peaks are observable for the minor form, probably due to the much lower intensity. The observations for **Eu-R-L3** are consistent with the solution state dynamics of  $[\text{Eu-DOTA}]^-$ . In **Eu-R-L3** the  $\Delta$  orientation of the

arms places the methyl group gauche to the lanthanide center creating strain in the system (Figure S1). We therefore expect the broad TSAP peaks to arise from the  $\Delta(\delta\delta\delta\delta)$  conformation. The rest of the forms can then be assigned based on the 2D EXSY spectrum and the peaks marked with green corresponds to  $\Delta(\lambda\lambda\lambda\lambda)$ , the peaks marked with pink to  $\Lambda(\delta\delta\delta\delta)$  and the TSAP giving rise to sharp signals, to the  $\Lambda(\lambda\lambda\lambda\lambda)$  form.

We note that **Eu-L2** and **Eu-L3** do not show forms induced by E/Z isomerism, suggesting that this is only apparent if the system is sterically congested i.e. in **[Eu-Bn-DOTAM]<sup>3+</sup>** or if both  $\alpha$  and  $\delta$  positions carry a chiral center.

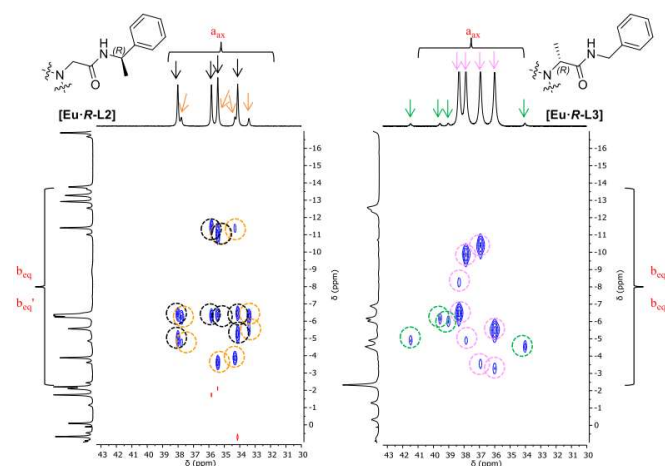


**Figure 9.** 2D EXSY spectra of **Eu-R-L2** (left) and **Eu-R-L3** (right) in MeOH-*d*<sub>4</sub> with a 12 ms mixing time.

## Conclusions

A series of chiral Eu-DOTA-monoamide complexes were synthesized, characterized, and their solution structures were explored using NMR spectroscopy. The addition of a chiral center in the  $\alpha$  or  $\delta$  positions on the amide pendant arm provided the expected result and resolved the four forms of the complexes in solution. Addition of chiral centers in both  $\alpha$  or  $\delta$  position resolved a second unexpected layer of complexity, which we had tentatively explained by the E/Z isomerism of the amide bond. The suggested E/Z isomerism of the amide was also likely present in the speciation of a Eu-DOTA-tetraamide complex.

The complexes of **Eu-L4** were used to model the effects that biological media impose on simple **[Eu-DOTA]<sup>3+</sup>** like complexes in solution. Even considering only the major form, all resonances in **Eu-L4** have been shifted compared to **Eu-L1**, **Eu-L2**, and **Eu-L3**. Thus, we must consider not only the new forms of the complex, but also that the properties of the dominating/original form will be perturbed.

We conclude that even the most robust of the kinetically inert lanthanide (III) complexes has a complicated speciation in biological media, and the differences in structure have the potential to significantly change the properties observed. While it will not be a surprise to the field, we here provide tangible evidence of the structural change

that can occur when a kinetically inert lanthanide complex is moved from a model system to a biological environment.

## ASSOCIATED CONTENT

**Supporting Information.** Detailed descriptions of General Methods, Synthetic Procedures, Conformation considerations, Experimental timescale consideration as well as NMR-Characterization, NMR experiments, and Computational details are supplied as Supporting.

## AUTHOR INFORMATION

### Corresponding Author

\* \*Department of Chemistry & Nano-Science Center, University of Copenhagen, Universitetsparken 5, DK2100 København Ø, Denmark, [tjs@chem.ku.dk](mailto:tjs@chem.ku.dk)

### Funding Sources

The Carlsberg Foundation, Villum Fonden, Novo Nordisk Fonden, Eliteforsk, and the University of Copenhagen. The Spanish Ministry for Science and Innovation and FEDER (grant PID2019-104626GB-I00) and Xunta de Galicia (Grant ED431B 2020/52)

## ACKNOWLEDGMENT

We thank the Carlsberg Foundation, Villum Fonden, Novo Nordisk Fonden, Eliteforsk, and the University of Copenhagen for generous support. C.P.-I. thanks the Spanish Ministry for Science and Innovation and FEDER (grant PID2019-104626GB-I00) and Xunta de Galicia (Grant ED431B 2020/52) for generous financial support.

## REFERENCES

1. G. Vereb, E. Jares-Erijman, P. R. Selvin and T. M. Jovin, *Biophysical Journal*, 1998, **74**, 2210-2222.
2. P. R. Selvin, *Annual review of biophysics and biomolecular structure*, 2002, **31**, 275-302.
3. M. C. Heffern, L. M. Matosziuk and T. J. Meade, *Chemical Reviews*, 2014, **114**, 4496-4539.
4. J.-C. G. Bünzli, *Chemical Reviews*, 2010, **110**, 2729-2755.
5. C. P. Montgomery, B. S. Murray, E. J. New, R. Pal and D. Parker, *Accounts of Chemical Research*, 2009, **42**, 925-937.
6. E. G. Moore, A. P. S. Samuel and K. N. Raymond, *Accounts of Chemical Research*, 2009, **42**, 542-552.
7. E. A. Akam, E. Abston, N. J. Rotile, H. R. Slattery, I. Y. Zhou, M. Lanuti and P. Caravan, *Chemical Science*, 2020, **11**, 224-231.
8. S. J. Butler, L. Lamarque, R. Pal and D. Parker, *Chemical Science*, 2014, **5**, 1750-1756.
9. A. T. Frawley, Holly V. Linford, M. Starck, R. Pal and D. Parker, *Chemical Science*, 2018, **9**, 1042-1049.
10. N. A. Thiele, V. Brown, J. M. Kelly, A. Amor-Coarasa, U. Jermilova, S. N. MacMillan, A. Nikolopoulou, S. Ponnala, C. F. Ramogida, A. K. H. Robertson, C. Rodríguez-Rodríguez, P. Schaffer, C. Williams Jr., J. W. Babich, V. Radchenko and J. J. Wilson, *Angewandte Chemie International Edition*, 2017, **56**, 14712-14717.
11. L. Dai, C. M. Jones, W. T. K. Chan, T. A. Pham, X. Ling, E. M. Gale, N. J. Rotile, W. C.-S. Tai, C. J. Anderson, P. Caravan and G.-L. Law, *Nature Communications*, 2018, **9**, 857.
12. P. Stachelek, L. MacKenzie, D. Parker and R. Pal, *Nature Communications*, 2022, **13**, 553.

13. A. Picot, A. D'Aléo, P. L. Baldeck, A. Grichine, A. Duperray, C. Andraud and O. Maury, *Journal of the American Chemical Society*, 2008, **130**, 1532-1533.
14. J.-M. Idée, M. Port, I. Raynal, M. Schaefer, S. Le Greneur and C. Corot, *Fundamental & Clinical Pharmacology*, 2006, **20**, 563-576.
15. A. Datta and K. N. Raymond, *Accounts of Chemical Research*, 2009, **42**, 938-947.
16. S. J. Franklin and K. N. Raymond, *Inorganic Chemistry*, 1994, **33**, 5794-5804.
17. S. L. Wu, S. J. Franklin, K. N. Raymond and W. D. Horrocks, *Inorganic Chemistry*, 1996, **35**, 162-167.
18. P. Caravan, J. J. Ellison, T. J. McMurry and R. B. Lauffer, *Chemical Reviews*, 1999, **99**, 2293-2352.
19. S. Aime, M. Botta, M. Fasano, M. P. M. Marques, C. F. G. C. Geraldes, D. Pubanz and A. E. Merbach, *Inorganic Chemistry*, 1997, **36**, 2059-2068.
20. D. Parker, R. S. Dickins, H. Puschmann, C. Crossland and J. A. K. Howard, *Chemical Reviews*, 2002, **102**, 1977-2010.
21. M. Woods, Z. Kovacs, S. Zhang and A. D. Sherry, *Angewandte Chemie*, 2003, **115**, 6069-6072.
22. J. A. K. Howard, A. M. Kenwright, J. M. Moloney, D. Parker, M. Woods, M. Port, M. Navet and O. Rousseau, *Chemical Communications*, 1998, DOI: 10.1039/A802847H, 1381-1382.
23. R. S. Ranganathan, R. K. Pillai, N. Raju, H. Fan, H. Nguyen, M. F. Tweedle, J. F. Desreux and V. Jacques, *Inorganic Chemistry*, 2002, **41**, 6846-6855.
24. R. S. Ranganathan, N. Raju, H. Fan, X. Zhang, M. F. Tweedle, J. F. Desreux and V. Jacques, *Inorganic Chemistry*, 2002, **41**, 6856-6866.
25. R. S. Dickins, J. A. K. Howard, C. L. Maupin, J. M. Moloney, D. Parker, J. P. Riehl, G. Siligardi and J. A. G. Williams, *Chemistry - A European Journal*, 1999, **5**, 1095-1105.
26. S. Shuvaev, E. A. Sutura, K. Mason and D. Parker, *Chemical Science*, 2018, **9**, 2996-3003.
27. S. Faulkner and O. Blackburn, in *The Chemistry of Molecular Imaging*, John Wiley & Sons, Inc, 2014, DOI: 10.1002/9781118854754.ch8, pp. 179-197.
28. E. Boros and P. Caravan, *Inorganic Chemistry*, 2015, **54**, 2403-2410.
29. E. Boros, S. Karimi, N. Kenton, L. Helm and P. Caravan, *Inorganic Chemistry*, 2014, **53**, 6985-6994.
30. S. Aime, A. Barge, M. Botta, A. S. D. Sousa and D. Parker, *Angewandte Chemie International Edition*, 1998, **37**, 2673-2675.
31. S. Aime, M. Botta, G. Ermondi, E. Terreno, P. L. Anelli, F. Fedeli and F. Uggeri, *Inorganic Chemistry*, 1996, **35**, 2726-2736.
32. S. Aime, M. Botta, Z. Garda, B. E. Kucera, G. Tircso, V. G. Young and M. Woods, *Inorganic Chemistry*, 2011, **50**, 7955-7965.
33. D. Delli Castelli, M. C. Caligara, M. Botta, E. Terreno and S. Aime, *Inorganic Chemistry*, 2013, **52**, 7130-7138.
34. M. Woods, S. Aime, M. Botta, J. A. K. Howard, J. M. Moloney, M. Navet, D. Parker, M. Port and O. Rousseau, *Journal of the American Chemical Society*, 2000, **122**, 9781-9792.
35. M. Woods, M. Botta, S. Avedano, J. Wang and A. D. Sherry, *Dalton Transactions*, 2005, DOI: 10.1039/B510778D, 3829-3837.
36. M. Woods, Z. Kovacs, R. Kiraly, E. Brücher, S. Zhang and A. D. Sherry, *Inorganic Chemistry*, 2004, **43**, 2845-2851.
37. L. Di Bari, G. Pintacuda and P. Salvadori, *Journal of the American Chemical Society*, 2000, **122**, 5557-5562.
38. L. Dai, W.-S. Lo, I. D. Coates, R. Pal and G.-L. Law, *Inorganic Chemistry*, 2016, **55**, 9065-9070.
39. P. R. Nawrocki, N. Kofod, M. Juelsholt, K. M. Jensen and T. J. Sørensen, *Physical Chemistry Chemical Physics*, 2020, **22**, 12794-12805.
40. S. Aime, E. Gianolio, E. Terreno, G. B. Giovenzana, R. Pagliarin, M. Sisti, G. Palmisano, M. Botta, M. P. Lowe and D. Parker, *JBIC Journal of Biological Inorganic Chemistry*, 2000, **5**, 488-497.
41. G.-L. Law, C. Man, D. Parker and J. W. Walton, *Chemical Communications*, 2010, **46**, 2391-2393.
42. J. F. Desreux, *Inorganic Chemistry*, 1980, **19**, 1319-1324.
43. A. Dadabhoy, S. Faulkner and P. G. Sammes, *Journal of the Chemical Society, Perkin Transactions 2*, 2002, DOI: 10.1039/b104541p, 348-357.
44. S. Aime, A. Barge, M. Botta, J. A. K. Howard, R. Kataký, M. P. Lowe, J. M. Moloney, D. Parker and A. S. de Sousa, *Chem. Commun.*, 1999, DOI: 10.1039/a902238d, 1047-1048.
45. M. Suchý, A. X. Li, M. Milne, R. Bartha and R. H. E. Hudson, *RSC Advances*, 2016, **6**, 62647-62655.
46. P. Goodrich, H. Q. Nimal Gunaratne, L. Hall, Y. Wang, L. Jin, M. J. Muldoon, A. P. C. Ribeiro, A. J. L. Pombeiro, V. I. Parvulescu, P. Davey and C. Hardacre, *Dalton Transactions*, 2017, **46**, 1704-1713.
47. F. W. Lewis, M. C. Eichler and D. H. Grayson, *Synlett*, 2009, DOI: 10.1055/s-0029-1217538, 1923-1928.
48. S. Liu, J. Pietryka, C. E. Ellars and D. S. Edwards, *Bioconjugate Chemistry*, 2002, **13**, 902-913.
49. A. K. R. Junker, M. Tropiano, S. Faulkner and T. J. Sørensen, *Inorganic Chemistry*, 2016, **55**, 12299-12308.
50. N. Cakić, B. Tickner, M. Zaiis, D. Esteban-Gómez, C. Platas-Iglesias and G. Angelovski, *Inorganic Chemistry*, 2017, **56**, 7737-7745.
51. N. Cakić, T. Savić, J. Stricker-Shaver, V. Truffault, C. Platas-Iglesias, C. Mirkes, R. Pohmann, K. Scheffler and G. Angelovski, *Chemical Communications*, 2016, **52**, 9224-9227.
52. S. Aime, M. Botta and G. Ermondi, *Inorganic Chemistry*, 1992, **31**, 4291-4299.
53. S. Hoeft and K. Roth, *Chemische Berichte*, 1993, **126**, 869-873.
54. L. G. Nielsen and T. J. Sørensen, *Inorganic Chemistry*, 2020, **59**, 94-105.
55. S. Hoeft and K. Roth, *Chemische Berichte*, 1993, **126**, 869-873.
56. J. Blahut, P. Hermann, Z. Tošner and C. Platas-Iglesias, *Physical Chemistry Chemical Physics*, 2017, **19**, 26662-26671.
57. L. S. Natrajan, N. M. Khoabane, B. L. Dadds, C. A. Muryn, R. G. Pritchard, S. L. Heath, A. M. Kenwright, I. Kuprov and S. Faulkner, *Inorganic chemistry*, 2010, **49**, 7700-7709.
58. V. Jacques and J. F. Desreux, *Inorganic Chemistry*, 1994, **33**, 4048-4053.
59. M. Regueiro-Figueroa, B. Bensenane, E. Ruscsák, D. Esteban-Gómez, L. J. Charbonnière, G. Tircsó, I. Tóth, A. d. Blas, T. Rodríguez-Blas and C. Platas-Iglesias, *Inorganic Chemistry*, 2011, **50**, 4125-4141.
60. U. Cosentino, A. Villa, D. Pitea, G. Moro, V. Barone and A. Maiocchi, *Journal of the American Chemical Society*, 2002, **124**, 4901-4909.
61. C. Platas-Iglesias, *European Journal of Inorganic Chemistry*, 2012, **2012**, 2023-2033.
62. O. A. Blackburn, J. D. Routledge, L. B. Jennings, N. H. Rees, A. M. Kenwright, P. D. Beer and S. Faulkner, *Dalton Transactions*, 2016, **45**, 3070-3077.
63. C. E. Carney, A. D. Tran, J. Wang, M. C. Schabel, A. D. Sherry and M. Woods, *Chemistry - A European Journal*, 2011, **17**, 10372-10378.
64. T. Mani, G. Tircsó, P. Zhao, A. D. Sherry and M. Woods, *Inorganic Chemistry*, 2009, **48**, 10338-10345.

65. L. G. Nielsen, A. K. R. Junker and T. J. Sorensen,  
*Dalton Transactions*, 2018, DOI: 10.1039/C8DT01501E.

